Received: 09-12-2013
Accepted: 01-01-2014

ISSN: 2321-4902
Volume 1 Issue 5

Online Available at www.chemijournal.com

International Journal of Chemical Studies

Thermal Analysis of Nalco Red Mud

S. N. Meher [1*]

1. National Aluminium Company Limited, Research & Development Department, M & R Complex, Damanjodi, Koraput-763008, Odisha, India .
[E-mail: shibnarayanmeher@gmail.com]

A NALCO red mud was thermally characterized. Chemical (major, minor and rare-earth elements) and mineralogical compositions were determined by XRF, ICP-MS and XRD techniques. The thermal events (TG/DTA/DSC) were observed in the range from room temperature to 1300 °C were related to the sample composition. The first mass loss step was related to free water content, while many of the other processes were related to dehydration processes. Three endothermic peaks were shown on DTA curve of red mud at temperature between 120-450 °C. The total mass loss in the red mud was found to be 12.70%, which was associated with moisture and water molecules in gibbsite, boehmite and diaspore phases. It was found that most of the decomposition reactions of hydrohematite, ferrihydrite, Aluminium goethite, boehmite, silicates and carbonates were strongly overlapping. It was also explained the formation of silicates and calcium titanate in between temperature range of 600-1000 °C which presence were confirmed by XRD. The ΔH for the decomposition of gibbsite and goethite and formation of silicates and calcium titanate are 102mJ/mg and 55.6mJ/mg respectively.

Keyword: Alumina, Red mud, Thermal, DTA and XRD

1. Introduction

Aluminium is a very important metal which is used everywhere from packing to aerospace industries. It is produced from alumina, using the Hall–Heroult cell [1-2]. Alumina is extracted from bauxite by the Bayer's process [3-4]. The process can be classified into five stages; mixing, digestion, precipitation, clarification and separation. In the digestion stage, gibbsite ($Al(OH)_3$) and boehmite ($AlO(OH)$) are dissolved in the mixture of bauxite and caustic soda, at temperature between105–108 °C, according to the reactions (1) and (2);

• Monohydrate alumina

$$Al_2O_3.H_2O + Na(OH).3H_2O = NaAl_2O_3(OH) + 4H_2O + \text{red mud (insoluble)} \quad (1)$$

• Trihydrate alumina

$$Al_2O_3.3H_2O + Na(OH).3H_2O = NaAl_2O_3(OH) + 6H_2O + \text{red mud (insoluble)} \quad (2)$$

Digestion stage is most important step in the Bayer's process. To yield high sodium aluminate solution depends on the used parameters in the digester. The solution of the sodium aluminate, $NaAl_2O_3(OH)$, commonly known as 'pregnant liquor', is cooled, diluted and seeded with aluminium three hydroxide($Al(OH)_3$, gibbsite) crystals (reaction: 3) and agitated for a period of time to precipitate the alumina which is then separated from the resulting spent liquor [4-5].

$$NaAlO_2 + 2H_2O = Na(OH) + Al(OH)_3 \quad (3)$$

The cream-colored aluminium hydroxide is thickened by the removal of water, before going to the calcinations stage, at over 1000 °C [5-6]. A fine, white powder of anhydrous alumina is formed. The following reaction (reaction: 4) gives the calcination operation:

$$Al_2O_3.3H_2O = Al_2O_{3(s)} + 3H_2O_{(g)} \quad (4)$$

Various gangue minerals, such as hematite, anatase, or rutile and desilication products (DSP) are not dissolved and remain as an insoluble solid phase which is, called red mud. DSP (desilication product) is a complex sodium aluminium-silicate waste of variable composition, which may include other oxides present in the solution. A typical desilication product is Sodalite which has an ideal formula $(NaAlSiO_4)_6.2NaX.0\text{-}6H_2O$ (where $X=Cl^-,OH^-,1/2CO_3^{2-},1/2SO_4^{2-},Al(OH)_4$). Iron oxide content gives its colour and liquid waste is red brown colour.

Chemical and mineralogical compositions are main importance for utilization of red mud for industrial applications. They determine any mechanical, physical properties and transformation reactions, which will take place during the heating of red mud. Thus, the potential use of red mud depend upon the chemical properties of the bauxite fed stock of the Bayer's process and this in turn is dependent on the geography of the area from which the bauxite is mined [4-7].

Mineral phase of red mud can be classified into two groups. Unchanged mineral phases of red mud come from the origin of bauxite ore without any transformation during the Bayer's process treatment. The old mineral phases are iron, titanium and un-reacted alumina phases. Formed phases are formed during the digestion stage as a result of the caustic soda addition. The studies on the utilization of red mud were started at the beginning of the alumina production. There are many investigations of looking at red mud as a new potential source for industrial applications [8–14], rather than the storage of it as a waste material. Due to the increasing environmental costs associated with the storage the utilization of red mud is economically more feasible for the recovery of both major and minor valuable metals in the red mud.

Pyro-metallurgy is imported process for production of many products. Final properties of any products depend on treatment parameters as well as compositions and mineral phases of used materials. To understand which mineral undergoes phase transformation and relationships between reactions, transformations and mineral phases, it is essential to know basic chemical and mineral compositions of raw materials. Differential thermal analysis is most common method for investigations of thermal properties and reactions, which may take place during the heating or cooling of sample. Any exothermic or endothermic reactions occur in sample during heating treatment can be observed on DTA curve. Generally, it is used at constant heating rate at around 5 °C min^{-1}.

Approximately 1-1.5 tons of bauxites residue is generated for production of 1 ton of alumina from the aluminium refinery plant of the world. The complete utilization of red mud and possibility of recovering valuable compound from red mud hasn't been investigated. The main objective of this study is to characterize the chemical and mineralogical compositions as well as thermal behavior of the NALCO red mud. It is necessary to know the thermal behavior of this material in order to design any manufacturing process. As the above study are also useful for the utilization of red mud for industrial application as well as evaluating the decomposition of mineral phases in red mud. Red muds from several sources have been studied by thermal analysis and other techniques. No data have been recorded on thermal characterization of NALCO red mud.

Table 1a: Chemical analysis of red mud (Major and minor elements)

Elements	Al_2O_3	Fe_2O_3	TiO_2	SiO_2	Na_2O	CaO	V_2O_5	MgO	MnO	LOI at 1000 °C
Range (%)	16-18	51-57	3-5	8-12	4-6	0.03-2.30	0.14-0.21	0.13-0.18	0.157-0.250	11-13
Typical (%)	16.07	53.75	4.24	8.25	3.82	1.48	0.148	0.020	0.157	11.83

2. Experimental

2.1 Material: Red mud (slurry) material was provided from the National Aluminium Company Limited, Damanjodi, Odisha. The plant obtained its bauxite from Panchapatmali Bauxite mines. Red mud sample was dried in an ordinary oven at

100°C for 12 h and then ground to 53-micron size by a pulverizer after proper coning and quartering. In this study the red mud was analyzed by chemical, X-ray fluorescence spectroscopy, atomic absorption spectroscopy X-ray diffraction, and scanning electron microscope with EDAX (SEM), BET surface area analyzer, laser particle size analyzer and thermal methods. To ascertain the elemental composition (major, minor and trace) of red mud, the red mud samples were analyzed by XRF, auto analyzer and ICP-MS techniques. The particle size distributions of red mud were determined by a Cilas-Model 1064 laser scattering particle size distribution analyzer. An amount of 0.1 g of sample powder was put in 100 ml of ethanol and underwent dispersion treatment by an ultrasonic dispersion unit for 60 s. The BET surface areas of red mud sample were determined in a Gemini 2360 surface area analyzer. An amount of 3 g of red mud sample was put in a glass tube and the sample was kept in de-gas unit at 105 ºC for 2 h to remove free moisture. The surface area, pore volume and pore diameter of red mud sample was then analyzed in BET surface areas analyzer in liquid nitrogen medium by flowing Helium and Nitrogen gas based on the principle of Langmuir adsorption theory applying free space correction method.

2.2 TG/DTA/DSC study

The thermal behaviors of the red mud were carried out by using simultaneous thermal analyzer (Model: Exstar 6300, Maker: Seikho, Japan). A Seikho instrument was used to record the differential scanning calorimeter (DSC), differential thermal analysis (DTA) curve and thermo gravimetric analysis (TG) curve. The experimental set up consisted of a heating ramp from 30–1200 °C at 5 °C min^{-1} followed by a cooling ramp from 1200-30 ºC at 5°C min^{-1}. About 15.13 mg of dried red mud sample was placed in platinum crucible on sample side. In the reference side 0.002 mg of alumina sample was placed in another platinum crucible to avoid analytical errors.

A red mud sample mass of 4.0 mg was placed in alumina crucible in sample side for DSC study while reference side remained empty. The experimental set up consisted of a heating ramp from 30–1300 °C at 5 °C min^{-1} followed by a cooling ramp from 1300-30 ºC at 5 °C min^{-1}. The thermal reactions were determined under nitrogen gas medium. In all experiments the flow rate of nitrogen gas was maintained at 50 mL min^{-1}.

2.3 SEM - EDAX study

The scanning electron microscope (Model: Leo 430, Maker: Leo, United Kingdom) was used to examine the surface and morphology of the NALCO red mud sample. Specimens were prepared by placing a little amount of red mud on aluminium holder using double-sided sticky tape and then they were coated with gold or palladium layer at 18mA for 105 second by vacuum evaporation (10^{-4} to 10^{-6} torr) as the red mud samples are not conductive. Energy disperse analysis of X-ray was used for the basic chemical analysis of the red mud sample. In this experiment, the prepared red mud sample was coated with gold by vacuum evaporation technique.

2.4 X-ray diffraction study

X-ray diffractometer (Model: dmax2200, Maker: Rigaku, Japan) was used for the determination of phases present in the red mud sample. The fine ground powder was compacted into the XRD sample holders. The obtained X-ray peaks were identified by comparison of the diffraction values and relative intensity obtained with those in the JCPDS file. The analysis was carried out at scan speed of 1º/min and scan step of 0.02 with 2θ value from 5 to 70º at 30 kV, 20 mA using CuKα radiation (Kα = 1.54186 Å with Nickel Filter) as an X-ray source.

3. Results and discussion

3.1 Characterization of the red mud

The X-ray diffraction pattern of the Nalco red mud sample is given in Fig. 1. The identified mineral phases in the sample are hematite (Fe_2O_3, card no. 33-0664 and d-value=1.70 Å and 2.52 Å), rutile (TiO_2, card no. 21-1276 and d-value=2.70 Å and 3.03 Å), perovskite ($CaTiO_3$, card no. 22-0153 and d-value=2.52 Å), quartz

(SiO_2 card no. 18-1166 and d-value=3.03 Å and 1.84 Å), sodalite ($Na_2O.Al_2O_3.SiO_2$, card no. 16-0612 and d-value=6.38 Å), boehmite {AlO(OH), card no. 21-1307 and d-value=2.62 Å}, goethite {FeO(OH), card no.260792 and d-value=2.43 Å, 2.52 Å and 4.15 Å },gibbsite {$Al(OH)_3$, card no. 33-180 and d-value=4.34 Å and 4.86 Å}, calcium alumina silicate {$Ca_2Al_2(SiO_4)(OH)_8$, card no. 03-0798 and d-value=3.69 Å and 6.38 Å}.

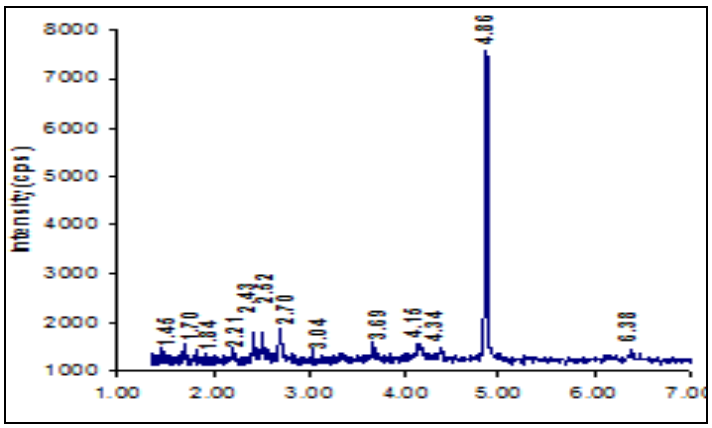

Fig 1: XRD pattern of NALCO red mud sample

Table 1 b: Chemical analysis of red mud (Trace elements and rare earth elements)

Trace elements		Rare-earths elements	
Elements	**In ppm**	**Elements**	**In ppm**
Sc	69.97	La	42.06
V	746.35	Ce	95.96
Cr	846.38	Pr	7.16
Co	22.14	Nd	18.65
Ni	45.91	Sm	3.36
Cu	103.86	Eu	0.83
Zn	86.57	Gd	3.48
Ga	93.17	Tb	0.33
Rb	5.99	Dy	2.10
Sr	47.66	Ho	0.29
Y	9.94	Er	0.82
Zr	234.13	Tm	0.13
Nb	40.07	Yb	0.99
Cs	0.25	Lu	0.14
Ba	90.77	-	-
Hf	8.28	-	-
Ta	2.57	-	-
Pb	48.28		-
Bi	38.08	-	-
Th	90.87	-	
U	1.56		

The basic chemical analysis of the red mud were given in table:- 1a and 1b. The major constituents of the NALCO red mud are Iron oxide (51-57%), aluminium oxide (16-18%), silicon dioxide (8-12%), sodium oxide (4-6%) and titanium oxide (3-5%) as shown in table:1a. Red mud contain several minor elements such as CaO, V_2O_5, MgO and MnO and trace amount of numerous elements such as oxides of P, Ga, Sc, V, Cr, Y, Zr, Nb, Cs, Hf, Ta, U, Th, Sr, Ba, Rb, K, Pb, Bi, Cu, Ni, Zn, Co as shown in table:-1b. It also contains rare earth elements in ppm level (i.e. La, Ce, Pr, Nd, Sm, Eu, Gd, Tb, Dy, Ho, Er, Tm, Yb, Lu) as shown in Table:1b. The presence of some trace

metals such as Cr (846ppm), V (746ppm), Zr (234ppm), Th and Ba (each 91ppm) in red mud in general is recorded. The SEM pictures of the red mud powder are shown in Fig. 2a nd Fig. 2b. As seen from this figure, the red mud composed of very fine particle size where the particle size ranges from a few microns to over 20 µm. Red mud is brick red in colour and slimy, having an average particle of less than 10 µm. The mean diameter of the precipitate was computed at 3 µm. About 35% by weight of solids contain less than 5 µm and about 80% less than 8 µm. It is alkaline, thixotropic, and possesses high surface area in the range of 13 - 20 m^2/g with a true density of 3.30 gm/cc, bulk density of 1.3 g/l and packed density 1.464 gm/cc**.** Red mud has a pore volume BJH of 0.086 cm^2/gm and average pore diameter BET 12.1 nm. Red mud powder has a variety of different morphology, some individual particle look flake, and spherical particles. There may be particle size differences between the unchanged with the new-formed mineral. The coarse particle would be belonging to the old mineral oxides. Red mud is distinctly alkaline having pH value of 10.0 to 12.7 with 15-30% solids. Sodium oxide content in the red mud sample is due to the addition of caustic soda for the recovery of aluminium content of the bauxite ore. It is possible to say that very fine particle may belong to sodium/aluminium minerals in the red mud powder. The large particle may belong to iron mineral groups or the unchanged minerals in the bauxite ore. SEM Micrographs show that the particles of red mud used were in poorly crystallized forms. Gibbsite was detected in the form of large hexagonal plate-like crystals with size from 5 µm to 20 µm (Fig.2a). Hematite presents globular structure and was detected in the form of aggregates of fine crystallites (Fig.2b). The aggregates had an irregular shape and a homogeneous size of about 5 µm (longest dimension). Iron and titanium corresponded to small granules, homogeneously distributed, while the larger flat particles present, mainly consisted of Al.

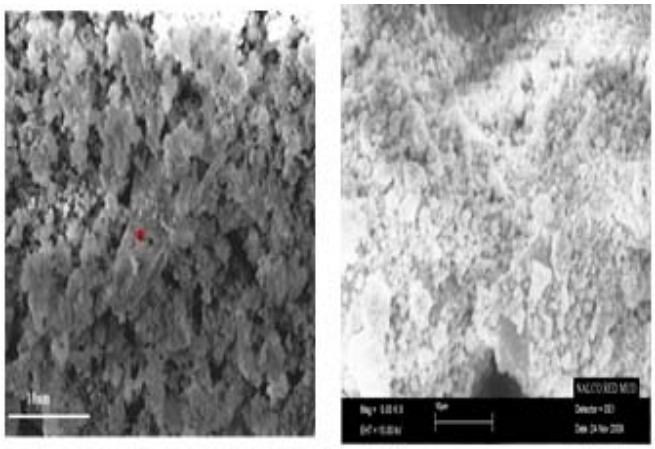

Fig 2a: and **Fig 2b:** SEM picture of NALCO red mud sample

Table 2: Common mineral phases of red mud

Formed phase	Phase form	Old phase	Phase form
Cal. Al. silicate	Ca2Al2(SiO4)(OH)8	Hematite Fe2O3	
Perovskite	CaTiO3	Goethite	FeO(OH)
Sodalite	$[NaAlSiO_4]_6$. 2NaX.0-6H_2O	Quartz	SiO2
Calcite	CaCO3	Boehmite	AlO(OH)
Sod. titanate	Na2TiO3	Rutile	TiO2
Cancrinite	$Ca_2Na_6[Al_6Si_6O_{24}](CO_3)_2.2H_2O$	Gibbsite	Al(OH)3
Al. silicate	—	Kaolinite Al4[Si4O10](OH)8	
		Ilmenite	FeO.TiO2

Table 3: Chemical analysis of bauxite and red mud

Chemical Constituents	(%)	(%)
Al_2O_3	44.41	16.07
SiO_2	3.14	8.25
Fe_2O_3	25.96	53.75
TiO_2	2.14	4.24
P_2O_5	0.1239	0.3450
V_2O_5	0.0655	0.1480
CaO	0.0078	1.4800
MnO	0.0732	0.1570
K_2O	0.0370	0.0990
ZnO	0.0070	0.0070
MgO	0.0070	0.0200
Ga_2O_3	0.0054	0.0850
Organic Carbon	0.0706	-
Mineral CO_3	0.1903	-
LOI	23.81	11.83

3.2 TG/DTA/DSC analysis

Since chemical compositions of bauxite and red mud vary (Table:-3), DTA curves of them will be different form. Red mud contains as many as 15-21 mineral phases (Table:- 2), such as gibbsite, goethite, boehmite hematite, kaolinite, sodalite/cancrinite, calcite, rutile, and quartz [15-20]. Thermal characteristics of red mud can vary sample to sample. For example, quartz is major oxide in many red mud, shows a small peak, as a result of α/β-transition at 570 °C. If kaolinite is major mineral phase in red mud sample, it shows nearly straight line.

There are different suggestions on the differential thermal analysis curve of gibbsite [21-23]. Atasoy [24] states that gibbsite shows an endothermic peak between 320–330 °C corresponding to a decomposition reaction forming *x*-Al_2O_3 on DTA curve. There may be small peak or inflection of variable size on peak within 250–300 °C range and small peak at temperature between 500–550 °C. The first peak is due to the formation of boehmite {γ-AlO(OH)} and the second peak is the dehydration of the formed boehmite phase. There is different approach on the DTA curve of gibbsite. According to Lodding [22], at constant heating rate, gibbsite partially dehydroxylates to boehmite a temperature 250 °C and the, remain part of the gibbsite goes to a transition alumina at about 330 °C. He suggests that, two separate endothermic peaks can be seen on DTA curve. According to Atasoy [23-24] observation, the decomposition of gibbsite, anhydrous alumina is formed and the dehydroxylation proceeds to the anhydrous alumina. But Lodding [22] suggests that, boehmite forms at the onset of dehydroxylation during this transformation and it forms a layer around the un-reacted gibbsite preventing further dehydroxylation until higher temperature is reached. The decomposition of gibbsite is given in the following equation 5.

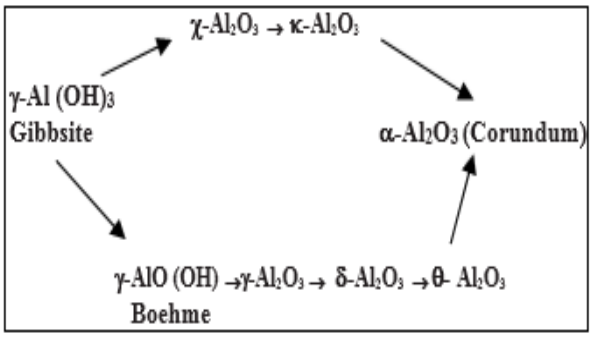

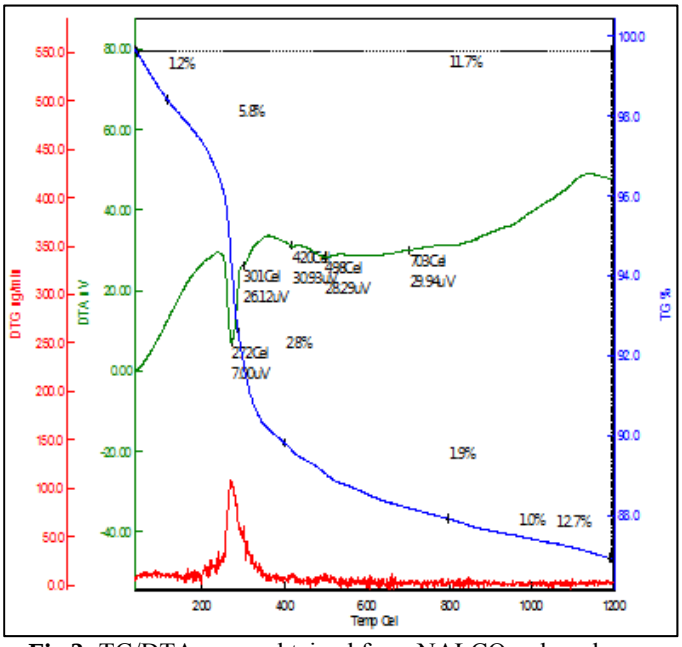

Fig 3: TG/DTA curve obtained from NALCO red mud sample

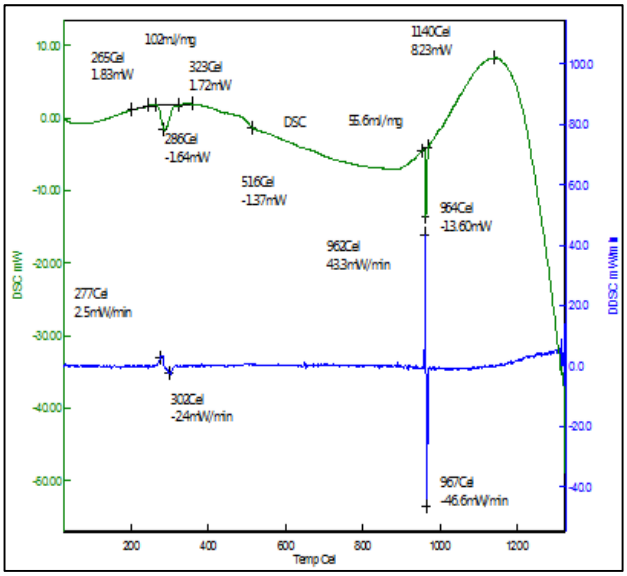

Fig 4: DSC curve obtained from NALCO red mud sample

There are several intermediate transition phases of alumina until to the α-Al_2O_3, corundum structure. All endothermic peaks of intermediate phases may not observe on the DTA curve.

However, the dehydration of goethite, FeO(OH),is more simple than gibbsite. Goethite decomposes to hematite and water as in the following equation;

$$\text{Goethite} \rightarrow \text{Hematite} + \text{Water(g)}$$

$$2\alpha FeO(OH)(s) \quad Fe_2O_3(s)+H_2O(g) \qquad (6)$$

Endothermic peaks on DTA can be explained with dehydration and decomposition of mineral phases in red mud. It is possible to observe formation of new phase and re-crystallization reactions as an exothermic peak on DTA curve.
The results of the differential thermal analysis (DTA) and thermal analysis (TG) of the red mud sample are given in Fig. 3. There are three endothermic peaks on the DTA. According to the above explanations, it is likely that for the NALCO red mud, the first two endothermic peaks between 272 and 301 °C, on the DTA curve, can be associated with the dehydration of gibbsite to form both boehmite and χ-alumina [9]. The third endothermic peak at 420 °C can be explained the decomposition of the goethite to hematite. The fourth endothermic peak at 498 °C was attributed to the decomposition of diaspore. Finally the low mass loss, without revealing a peak, occurring after 805 °C can be related to sodium aluminum carbonate silicate decomposition in the red mud. The two exothermic peaks in the temperature range of 200-400 °C is due to decompositions of gibbsite and boehmite from red mud.

The result of the thermo gravimetric analysis (TG) of the red mud sample is given in Fig. 3. It can be seen from the TG curve, there is very little mass loss up to 120 °C in the red mud sample. But the mass loss of the sample is very rapid between 120–450 °C. There are three endothermic peaks on DTA curve of the sample within this temperature range. The mass loss observed of the sample was 1.2%, which can be explained with the loss of physical water content of the sample. There is also very rapid mass loss in the sample at 272–301 °C temperature range. The mass loss is associated with the loss of water from the gibbsite (5.8%) and goethite (2.8%) phases. The mass loss is associated with the loss of water from the diaspore (1.9%) and loss of CO_2 both from the calcite and sodium aluminum carbonate silicate (1.0%) phases. The total mass loss of the red mud is 12.70% until 1200 °C. It is good agreement with the DTA curve of the sample. The endothermic peaks came cross to loose of water from gibbsite and goethite phases.

The DSC trace of NALCO red mud in Fig. 4 shows that at 266 °C begins an endothermic effect that ends around 1140 °C. The ΔH for the decomposition of decomposition of gibbsite and goethite is 102mJ/mg as shown in DSC plot (Fig.4). Taking into account the initial composition of the sample, it is likely that around 580°C begins the following endothermic reaction [25]:

$$Na_2CO_3+CaCO_3 \rightarrow Na_2Ca(CO_3)_2.$$

At 680 °C this compound can start to react with the silica present in the sample producing the following substances:

$2[Na_2O{\cdot}2SiO_2]+[Na_2O{\cdot}3CaO{\cdot}6SiO_2]$, what is also an endothermic process associated with mass loss [25]. This process was reported to end at 830 °C [26–28].

In the range from 600 to 1000 °C, it is also likely that it takes place the formation of $Na_2SiO_3+CaSiO_3$.

The endothermic peak observed at 964°C is probably due to peritectic melting of calcium disilicate, which can react in liquid phase [25]:

$$[Na_2O{\cdot}3CaO{\cdot}6SiO_2]+[Na_2O{\cdot}2SiO_2] \rightarrow$$
$$\rightarrow [Na_2O{\cdot}2CaO{\cdot}3SiO_2]+ \text{líquidus}$$

It was reported that calcium carbonate decomposition takes place between 680 and 776 °C [21], and, in the case of other red muds, between 560 and 720 °C [30]. The calcium carbonate present in the sample is expected to decompose in this range of temperature. The CaO resulting from the calcium carbonate decomposition may react with titanium oxide [25]:

$$CaO+TiO_2 \rightarrow CaTiO_3$$

This reaction was confirmed by the presence of calcium titanate at 1140 °C, which was not present in the original sample. The reaction of formation of $CaTiO_3$ from CaO and TiO_2 is exothermic, but there is no exothermic peak on the DSC curve that can confirm that this reaction occurred. The exothermic peak on DSC curves is probably hidden under the endothermic peak of $CaCO_3$.

Silicates formation was also reported for the range from 600 to 1000 °C, overlapping with the calcium carbonate decomposition [25]: The ΔH for the formation of silicates and calcium titanate is 55.60 mJ/mg as shown in DSC plot (Fig.4).

$$Na_2CO_3+SiO_2 \rightarrow Na_2SiO_3+CO_2(g)$$

$$2CaCO_3+SiO_2 \rightarrow Ca_2SiO_4+2CO_2(g)$$

$$Ca_2SiO_4+SiO_2 \rightarrow 2CaSiO_3$$

Other process that can be responsible of the very slow mass change that continues at temperature above 400 °C is the residual hydrohematite dehydration. Only part of hydrohematite dehydrates at 160–200 °C [29]. It was reported that small quantities of water in this species resist heating even at 1000 °C [31]. There is an endothermic peak above 1200 °C that can be attributed to melting of some of the silicates (sodalite) present at that temperature.

Figure 4 plots an overlay of the heat flow plots obtained during the first and second heating-cooling cycles. The sample mass did not change after completion of the first heating scan. It means that no dehydration or decomposition occurred beyond the first heating scan. The first cooling DSC trace shows an exothermic peak at around 1140 °C. It is compatible with some crystallization processes. The second heating and cooling ramps gave again these peaks. It confirms the hypothesis of melting at 1140 °C during the heating ramp and crystallization during the cooling ramp at 1100 °C in a crystalline form. No other noticeable thermal events were found.

4. Conclusions

The Nalco red mud sample was characterized. Following statements can be made up on the results: -

1) It was very fine-grained powder having median diameter (D_{50}) of 3 µm with true density of 3.30 g cm^{-3} and packed density 1.464 gm/cc and ready to any mineral processing and separation.
2) It possesses high surface area in the range of 13-20 m^2/g. It has a pore volume BJH of 0.086 cm^2/gm and average pore diameter BET 12.1 nm.
3) It contains considerable amount of the valuable oxides, iron, titanium and aluminium hydroxides. Total iron oxide content of the sample is 51-57%. It is reducible and can be separated by smelting, solid-state reduction or DRI process and magnetic separation techniques.
4) The un-recovered sodium aluminate content is very high in the sample. The recovery of aluminium hydroxides can increase by

improving the washing conditions or the re-washing of the red mud slurry. SiO_2 is third major phase with 8-12% content.

5) It contain several minor elements such as CaO, V_2O_5, MgO and MnO and trace amount of numerous elements as oxides of P, Ga, Sc, V, Cr,Y, Zr, Nb, Cs, Hf, Ta, U, Th, Sr, Ba, Rb, K, Pb, Bi, Cu, Ni, Zn, Co Rare earth elements in ppm level (i.e. La, Ce, Pr, Nd, Sm, Eu, Gd, Tb, Dy, Ho, Er, Tm, Yb, Lu). Enrichment in some trace metals such as Cr (846ppm), V (746ppm), Zr (234ppm), Th and Ba (each 91ppm) in red mud in general is recorded.
6) Hematite presented globular structure and was detected in the form of aggregates of fine crystallites (5 µm) where as Gibbsite (5 µm to 20 µm) was detected in the form of large hexagonal plate-like crystals in red mud.
7) Two exothermic peaks and three endothermic peaks were determined on the DTA curve of the red mud sample at temperature range of 120–450 °C and 12.70% of the total mass loss was observed on the TG of the sample.
8) It was also explained from the DSC curve of red mud that the formation of silicates and calcium titanate in between temperature range of 600-1000 ºC which presence was confirmed by XRD. The ΔH for the decomposition of gibbsite and goethite and formation of silicates and calcium titanate are 102mJ/mg and 55.6mJ/mg respectively.

5. Acknowledgements

The authors are gratefully thankful to Management of National Aluminium Company Limited for their support and kind permission for publishing this research article.

6. References

1. Hall CM, US Patent No: 400 667.
2. Heroult R, French Patent No: 175 711.
3. Bayer K J, German Patent No: 2150677.
4. Parekh BK, Proc. of 6th Min. Waste Utilization Symp, 1978; 6: 123.
5. Prasad PM, Sharma JM, Electrometallurgy, Conf. Proc. 1986.
6. Wagh AS, Douse VE, J. Mater. Res. 1991; 6: 1094.
7. Wagh AS, Bauxite Tailing, Proc. Inter. Conf., Jamaica 1986; 156.
8. Parekh BK, Goldberger WM, 1976; Report No: 600/2-76-301.
9. Frusman OG, Mauser JF, Butler MO, Stickney WA, 1970; US Report No. 7454
10. US Patent 5008089, 1991.
11. Puskas F. Bauxite Tailing, Proc. Inter. Conf., Jamaica 1986; 127.
12. Kornyei J, Teribesi L, J. Scin. Ind. Res. 1983; 42:456.
13. Atasoy A, MAMTEK 2002-Turkey.
14. Merkin L, Ph.D. Thesis, Manchester University, 1996.
15. Parekh BK, Goldberger WM, 1976, Report No. EPA-600/2-76-301, Ind. Env. Lab., US EPA, Cincinnati.
16. Prasad PM, Proc. of Met. Sci.- The Emerging Frontiers (ICMS-77). eds Anantharaman TR, Malhotra SL, Ranganathan Sand Rama Rao P, Indian Inst. Metals, Calcutta. 1979; 461:478.
17. Prasad PM, Kachhawaha JS, Gupta RC, Mankhand TR, Sharma JM, Proc. of Light Metals: Science and Technology, Trans. Tech. Publications Ltd., Switzerland. 1985; 31:52.
18. Prasad PM, Sharma JM, Proc. of Electrometallurgy, Cent. Electrochemical Res. Inst., Karaikudi, India, 1986; 12:23.
19. Venugopal TA, Sharma JM, Prasad PM, Proc. Int. Conf. Bauxite Tailings "Red mud", eds Wagh AS, Desai P, The Jamaica Bauxite Institute and The Univ. of the West Indies, Kingston, Jamaica. 1987; 137:141.
20. Sharma JM, Ph. D (Met. Engg.) Thesis, Banaras Hindu University, Varanasi, India. 1990.
21. Alp A, Goral S, J. Therm. Anal. Cal. 2003; (73): 201-207.
22. Lodding W, Thermal Analysis, Academic Press, London. 1969.
23. Atasoy A, MSc. Dissertation, UMIST. 1996.
24. Atasoy A, Journal of Thermal Analysis and Calorimetry. 2007; 90(1): 153-158.
25. Jordán R, Faria T, Rodríguez G, César-Díaz G, Zayas ME, Ingeniería y Ciencía. 2007; 3: 91.
26. La Course WC, The Glass Researcher. 2001; 18.
27. Brüning R, Sutton M, J. Non-Crystalline Solids, 1996; 205:480.
28. Webb T L, Heystek H, The carbonate minerals. In: Mackenzie RC, Editor, The Differential Thermal Investigation of Clays, Mineralogical Society, London 1957; 329: 363.
29. Kurnakow NS, Rode EJ, Zeitschrift füranorganische und allgemeine Chemie, 1928; 169:57.
30. Liu Y, Lin Cand, Wu Y, J. Hazard Mater, 2007; 146:255.
31. Wolska E, Kristallogr Z, 1981; 154:69.